Monthly Notices
of the
ROYAL ASTRONOMICAL SOCIETY

MNRAS **483,** 3730–3737 (2019)
Advance Access publication 2018 December 10

doi:10.1093/mnras/sty3348

Radial evolution of the solar wind in pure high-speed streams: HELIOS revised observations

Denise Perrone [1]★ D. Stansby [1] T. S. Horbury [1] and L. Matteini [2]

[1] *Department of Physics, Imperial College London, London SW7 2AZ, UK*
[2] *LESIA, Observatoire de Paris, Université PSL, CNRS, Sorbonne Université, Univ. Paris Diderot, Sorbonne Paris Cité, 5 Place Jules Janssen, 92195 Meudon, France*

Accepted 2018 December 6. Received 2018 November 16; in original form 2018 October 5

ABSTRACT

Spacecraft observations have shown that the proton temperature in the solar wind falls off with radial distance more slowly than expected for an adiabatic prediction. Usually, previous studies have been focused on the evolution of the solar-wind plasma by using the bulk speed as an order parameter to discriminate different regimes. In contrast, here, we study the radial evolution of pure and homogeneous fast streams (i.e. well-defined streams of coronal-hole plasma that maintain their identity during several solar rotations) by means of re-processed particle data, from the HELIOS satellites between 0.3 and 1 au. We have identified 16 intervals of unperturbed high-speed coronal-hole plasma, from three different sources and measured at different radial distances. The observations show that, for all three streams, (i) the proton density decreases as expected for a radially expanding plasma, unlike previous analysis that found a slower decrease; (ii) the magnetic field deviates from the Parker prediction, with the radial component decreasing more slowly and the tangential more quickly than expected; (iii) the double-adiabatic invariants are violated and an increase of entropy is observed; (iv) the collisional frequency is not constant, but decreases as the plasma travels away from the Sun. This work provides an insight into the heating problem in pure fast solar wind, fitting in the context of the next solar missions, and, especially for Parker Solar Probe, it enables us to predict the high-speed solar-wind environment much closer to the Sun.

Key words: Sun: corona – Sun: heliosphere – solar wind.

1 INTRODUCTION

The puzzle of ion acceleration and heating of the solar wind is one of the most compelling problems in space plasma physics, since no direct measurements exist in the region where these processes actually occur. In this context, the next solar missions, NASA's Parker Solar Probe (Fox et al. 2016) and ESA's Solar Orbiter (Muller et al. 2013), will give a crucial contribution. To date, the only missions specifically designed to explore the interplanetary medium in the near-solar environment were the HELIOS solar probes (Schwenn and Marsch 1990) which provided, for the first time, full three-dimensional ion velocity distributions. These displayed, especially in fast solar wind, strong departures from thermodynamic equilibrium. In particular, the core (which contains about 80 per cent of the proton population) showed a strong anisotropy with respect to the background magnetic field (Marsch et al. 1982; Bourouaine, Marsch & Neubauer 2010). In addition, a proton field-aligned beam, whose relative speed with respect to the core is of the order of the local Alfvén speed (Marsch et al. 1982), is often observed. Moreover, the proton temperature is observed to fall off more slowly than expected for an adiabatic prediction during the radial evolution of the wind, highlighting the need for additional heating in order to explain the observations.

In a collisionless and anisotropic plasma, like the solar wind, the variation of the parallel, $T_{\parallel}$, and perpendicular, $T_{\perp}$, temperatures should be described (neglecting collisions and heat fluxes) by the double-adiabatic hypothesis (Chew, Goldberger & Low 1956). For a spherical expansion, in the presence of a strictly radial magnetic field and a constant velocity, $T_{\perp}$ should decrease as R^{-2} and $T_{\parallel}$ should not change. However, *in situ* measurements showed that these invariants are broken (Marsch et al. 1983), due to the action of turbulent dissipation or wave damping (Marsch & Richter 1987), with $T_{\perp}$ decreasing more slowly and $T_{\parallel}$ decreasing faster, than expected (Marsch et al. 1982; Hellinger et al. 2011, 2013). Some of the observed properties are compatible with the interaction of the ions with high-frequency Alfvén-cyclotron waves (e.g. Hollweg & Isenberg 2002). Signatures of cyclotron heating with the formation of quasi-linear plateaux are also observed (Heuer & Marsch 2007). Moreover, there is evidence of heating associated with the turbulent

★ E-mail: d.perrone@imperial.ac.uk

cascade (Breech et al. 2009; Cranmer et al. 2009). Finally, the departure from isotropy is also a possible source of free energy. In particular, in fast wind, the proton-cyclotron instability (Gary et al. 2001) or the mirror-mode instability (Hellinger et al. 2006) could shape the proton distribution function.

The complex shape of the ion velocity distributions suggests that Coulomb collisions are not able to keep the system in thermodynamic equilibrium. However, the role of collisions depends on the properties of the wind and varies with distance and latitude (Matteini et al. 2012). In particular, collisions influence the ion velocity distributions in slow solar wind (Livi, Marsch & Rosenbauer 1986), working to remove anisotropies and the relative proton-alpha drift, while their role in fast wind can be considered negligible (Marsch & Goldstein 1983). On the other hand, in fast wind, the observed temperature anisotropy cannot be described through a purely collisionless expansion, meaning that wave-particle interactions or heat conduction must play a role.

An accurate classification of the wind is crucial in order to understand and interpret the observations. Recent categorizations discern the solar wind by its origin (e.g. Camporeale, Carè & Borovsky 2018; Stansby, Horbury & Matteini 2019), considering the classification based on the particle speed too simplistic. However, most of the studies on its radial evolution in different regimes have been performed using the bulk speed as an order parameter, i.e. by using a threshold for the proton radial velocity (Hellinger et al. 2011, 2013) or averages over 100 km s^{-1} wide speed intervals (e.g. Marsch et al. 1982). Unfortunately, both these choices can be limited and approximate, since streams with different origins or from heterogeneous solar-wind types could be taken together, potentially leading to erroneous conclusions. In this respect, an ideal approach is to use a well-defined stream that maintains its identity during the radial expansion. A high-velocity stream, observed by HELIOS spacecraft during three successive solar rotations and at different distances from the Sun, has been used to study the radial evolution of MHD power spectra by means of magnetic field data (Bavassano et al. 1981, 1982a,b), where the intervals have been selected by visual inspection of hourly averaged data.

High-speed streams, originating in coronal holes, are always present in the heliosphere (Hundhausen 1972; Geiss, Gloeckler & Von Steiger 1995). While fast streams have fairly steady velocity, it still varies on large (hours) scales, which makes identification of the edges difficult. Smaller scale variations are also present, including the recently identified enhancements in plasma speed in one near-Sun fast stream (Horbury, Matteini & Stansby 2018). These events are Alfvénic and the proton core distribution within them is no different to the background wind (Matteini et al. 2014). Moving radially outwards, high-speed wind interacts with the preceding slower wind, forming a region of compressed plasma along the leading edge of the stream. Moreover, the boundary between slow and fast wind is typically characterized by a sharp density drop, temperature rise, and specific entropy increase (Richardson 2018).

In this paper, we study the radial evolution of pure and homogeneous high-speed streams in the inner heliosphere. In order to avoid any additional effects due to the presence of interaction regions (e.g. acceleration/deceleration of the streams), we select only intervals of unperturbed coronal-hole plasma, from different sources, and we follow their radial evolution during several solar rotations.

2 HIGH-SPEED PLASMA STREAMS

We use data from the twin HELIOS probes in the first 2 yr of their mission, which correspond to a declining phase of solar activity when the interplanetary structure was characterized by stable recurrent high-speed streams (Fig. 1). The study is performed on a new data set (Stansby 2017; Stansby et al. 2018) which contains estimates of number density, velocity and temperatures of the proton-core population, obtained from a systematic fitting with bi-Maxwellian functions of all the original HELIOS 3D distribution functions. Magnetic field data are also provided as an average from the values taken whilst the distribution function was measured.

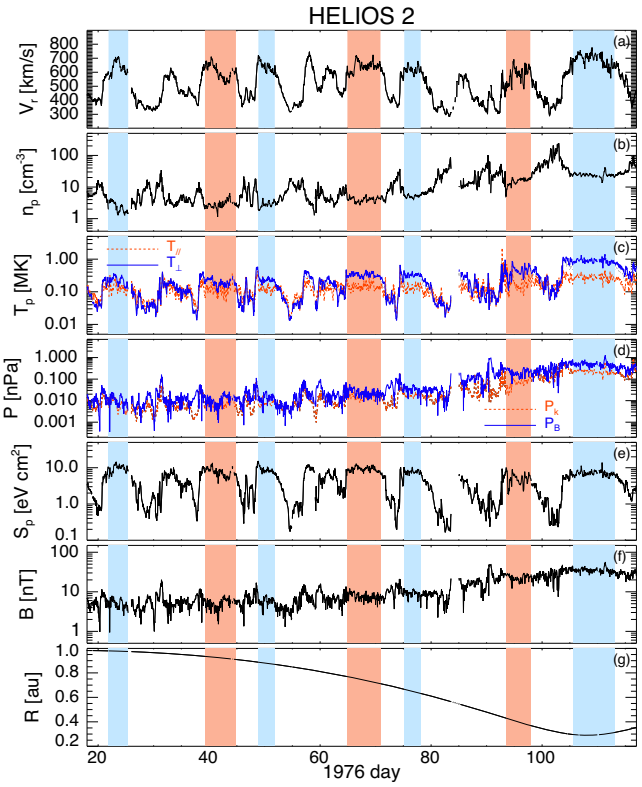

Figure 1. Hourly averaged HELIOS2 solar-wind data. (a) Radial component of the velocity; (b) proton density; (c) proton temperature: $T_{//}$ (red-dashed) and $T_\perp$ (blue-solid); (d) proton kinetic pressure, $P_k = n_p k_B T_p$ (red-dashed), and magnetic pressure, $P_B = B^2/8\pi$ (blue-solid line); (e) proton specific entropy; (f) magnitude of the magnetic field; and (g) radial distance. Colour-filled bands denote unperturbed coronal-hole plasma streams. Different colours indicate recurrent streams of different origin.

Here, rather than taking a cut-off in speed, we select more restricted periods within high-speed streams (Borovsky 2016), characterized by a 'flat-top-like' shape in the temporal profile of the solar-wind velocity and approximately constant values for the magnetic field strength, proton density and specific entropy, $S_p = T_p/n_p^{2/3}$. This avoids compressed coronal-hole plasma, at the end of the corotating interaction regions, and rarefaction regions, on the trailing edge of high-speed streams. An example of the identification procedure is shown in Fig. 2.

Following Borovsky (2016), the onset of the unperturbed coronal-hole interval is chosen when the magnetic field (green-triangle line) and the proton density (violet-star line) decline to more or less steady values early in the flattop region. Moreover, at the same time, the proton specific entropy (orange-diamond line) reaches a maximum and steady value. The end of the interval, which corresponds to the onset of the rarefaction region, is taken when the solar-wind velocity starts to systematically decrease and also the proton specific entropy starts to decline from high (and steady) values towards

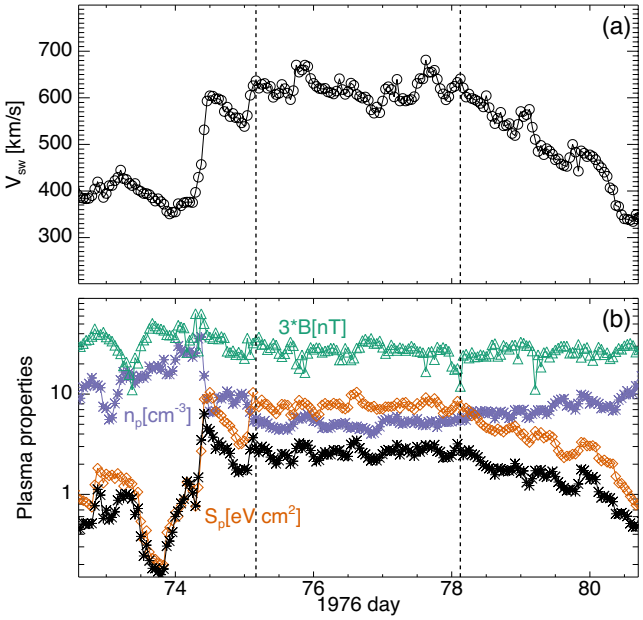

Figure 2. Example of unperturbed coronal-hole plasma. Hourly averaged data of solar-wind speed in panel (a), and proton density (violet-star line), magnetic field (green-triangle line), and proton specific entropy (orange-diamond line) in panel (b). Vertical black-dashed lines indicate onset and end of the flattop, respectively.

Table 1. Intervals of unperturbed coronal-hole plasma in both HELIOS1 and HELIOS2 used in this study.

		Start		End			
Spacecraft	Year	Day	UT	Day	UT	R (au)	Flattop
HELIOS1	1975	13	04	17	02	0.88	C1
HELIOS1	1975	40	08	45	21	0.64	C2
HELIOS1	1975	72	16	75	02	0.31	C3
HELIOS1	1975	306	08	308	00	0.76	A1
HELIOS1	1975	359	12	361	10	0.99	A2
HELIOS2	1976	21	21	25	10	0.98	A3
HELIOS2	1976	39	06	44	20	0.92	B1
HELIOS1	1976	47	02	49	14	0.74	A4
HELIOS2	1976	48	21	51	20	0.88	A5
HELIOS2	1976	64	22	70	21	0.74	B2
HELIOS1	1976	65	20	70	11	0.53	B3
HELIOS1	1976	74	10	79	13	0.42	A6
HELIOS2	1976	75	04	78	03	0.65	A7
HELIOS2	1976	94	16	97	21	0.40	B4
HELIOS2	1976	105	14	113	01	0.30	A8
HELIOS1	1976	113	10	116	21	0.57	A9

lower values. The same behaviour of S_p is also observed for the proton temperature (not shown here). Between 1975 January and 1976 April, we identify 16 intervals of unperturbed coronal-hole plasma, from three different coronal holes and at different radial distances. The streams are listed in Table 1, where the different origin is indicated with different letters, while the number indicates the chronological order. Recurrent flattops originating in the same coronal hole allow the investigation of the radial evolution in a homogeneous dataset of pure fast wind, assuming that variations with heliographic latitude are absent or not important. Therefore, it is possible to study the plasma evolution from the same region as it evolves with distance. Finally, the presence of three homogeneous

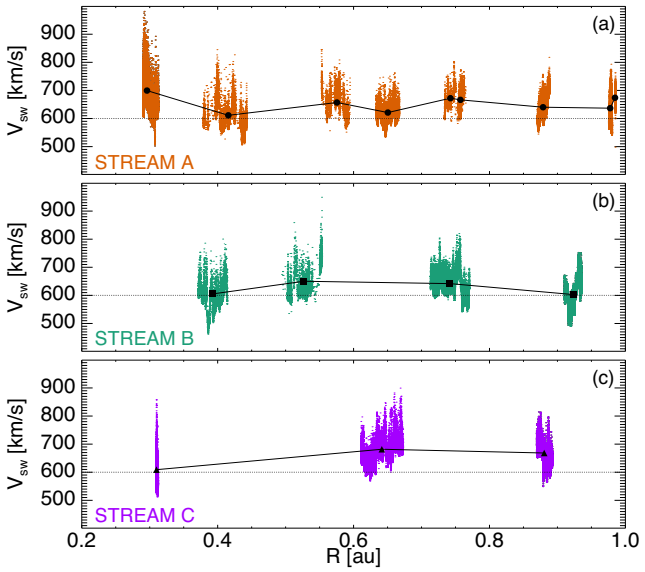

Figure 3. Solar-wind speed, V_{sw}, for the three recurrent flattop streams as a function of the radial distance, R. The black symbols indicate the mean of the speed in each interval listed in Table 1, while the horizontal dotted lines refer to the threshold used by Hellinger et al. (2011) to select fast wind.

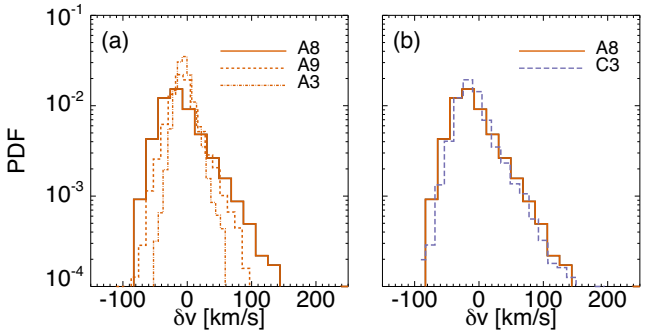

Figure 4. Probability distribution functions of the radial speed with respect to a 30 min running mean during (a) three flattops of the same stream at different radial distances, $R \sim 0.3$, 0.57, 0.98 au, and (b) two flattops of different streams at ∼0.3 au.

intervals, from three different coronal holes, allows us to study the dependence on the source of the high-speed streams.

The solar-wind speed in each stream (Fig. 3) can have a wide range of values, sometimes surprisingly low. Stream B, for example, has flattop intervals with V_{sw} much lower than 600 km s^{-1} (horizontal dotted lines), but is still a high-speed stream. This means that fixing a low threshold in speed for selecting fast wind, as in the case discussed in Hellinger et al. (2011), can give incomplete information. Moreover, knowing the value of the velocity without the context of the observation can give approximate and eventually erroneous information, since high values of the velocity (i.e. $V_{sw} > 600$ km s^{-1}) can be also associated with interaction regions, which have different physics with respect to pure fast streams. Furthermore, the choice to bin the speed in range of 100 km s^{-1} (e.g. Marsch et al. 1982) can mix wind from different sources or interaction regions, since the value of the velocity cannot be used alone to discriminate between different types of wind.

Fig. 4 shows the probability distribution functions (PDFs) of the instantaneous radial velocity fluctuations with respect to a 30 min

running average speed, i.e. $\delta v = V_r - \langle V_r \rangle$. The PDF of δv for the flattop A8, which includes the high-speed stream studied by Horbury et al. (2018), is indicated in both panels by a solid-orange line and is characterized by a longer right tail (positively skewed). In panel (a) we compare this PDF (at $R \sim 0.3$ au) with the PDF of two other flattops of the same stream but at different radial distances, i.e. flattop A9 ($R \sim 0.57$ au, orange-dashed line) and flattop A3 ($R \sim 0.98$ au, orange-dash–dotted line). The spikes have lower amplitudes as the stream moves away from the Sun (see also Matteini et al. 2014) and also the skewness of the distributions becomes less important (at 1 au the distribution is almost symmetric). In panel (b) we show the comparison between the flattop A8 and a flattop from a different stream (C3, violet-long-dashed line) but at the same distance from the Sun ($R \sim 0.31$ au). In this case, the PDFs are similar, meaning that the importance of the spikes is characterized by the distance from the Sun and is independent of the origin of the specific stream. Moreover, if we analyse the PDFs of δv normalized to the mean value of the Alfvén speed within each interval (not shown here), we find that they are all comparable. Therefore, the amplitude of the spikes is constrained by the Alfvén speed, as expected due to their Alfvénic nature (Matteini et al. 2015). Finally, our results suggest that the spikes are a general feature of the near-Sun high-speed environment.

3 RADIAL DEPENDENCES

We study the radial evolution of the three unperturbed coronal-hole high-speed streams listed in Table 1. In Figs 5 and 6, we fit (black-solid lines) the averaged values of stream A by using the least-squares linear regression function (although for some of the considered quantities no power law is expected) in logarithmic space, $\log f = \alpha \log x + k$, with $x = R/R_0$ ($R_0 = 1$ au) and $k = \log f_0$. In principle, the least-square linear regression in logarithmic space could alter the error of the distribution. However, a linear fit gives almost the same results with respect to a least-square non-linear regression, where a power-law dependence is used, in agreement with Hellinger et al. (2013). The choice of stream A is only due to statistical reasons (i.e. it is the stream with the most intervals) and does not influence the generality of the results since most of the points of the other streams lie on the same line. Moreover, comparisons with previous studies and/or with theoretical predictions are shown (see legends), although we look only at the proton-core population while most of the studies used for the comparison are based on the moments of the full proton distribution. Finally, expected values in fast streams at $\sim 35 R_s$ (blue-filled band), where R_s is the solar radius, which corresponds to the heliospheric distance of the first three perihelia for Parker Solar Probe, are indicated by blue stars.

3.1 Proton density and magnetic field

The radial dependence of the proton number density, n_p, shown in Fig. 5(a), is

$$n_p = (2.4 \pm 0.1)(R/R_0)^{-(1.96 \pm 0.07)} \text{ cm}^{-3}. \quad (1)$$

Unlike that found by Hellinger et al. (2011), i.e. $n_p \propto R^{-1.8}$, indicated as a black-dashed line (assuming the same density at $R = 1$ au to show how they diverge at smaller R), the proton-core density decreases as expected for a radially expanding solar wind. Moreover, the density flux, $n_p V_r R^2$, is almost constant, where the fit for stream A is $n_p V_r \propto R^{-(1.97 \pm 0.08)}$. This implies that no protons are removed from or added to the core.

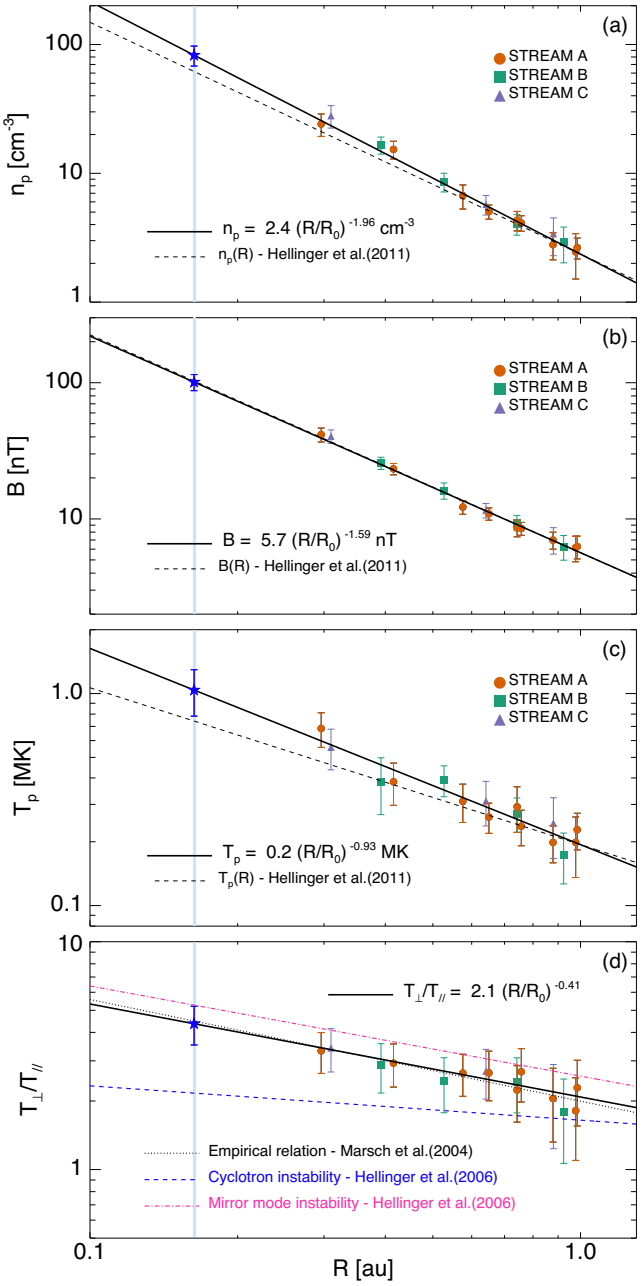

Figure 5. Solar-wind radial evolution: (a) proton density; (b) magnetic field magnitude; (c) proton temperature; and (d) temperature anisotropy. Each point and relative error bar refer to the mean and ± the standard deviation in each flattop. Different colours and symbols indicate different streams. Black-solid lines show the fits for the stream A (orange circles). Blue stars refer to extrapolated fast-stream values at $\sim 35 R_s$ (blue-filled band).

Fig. 5(b) shows the radial evolution of the magnetic field magnitude, B, where the fit is

$$B = (5.7 \pm 0.2)(R/R_0)^{-(1.59 \pm 0.06)} \text{ nT}. \quad (2)$$

The same dependence, $B \propto R^{-1.6}$, was found in Hellinger et al. (2011). According to the Parker model (Parker 1958, 1963), the radial component of the magnetic field should decrease as R^{-2}, while the tangential component should vary as R^{-1}. Here, in a minimum phase of solar activity (i.e. the coronal magnetic field is largely dipole-like) and for pure high-speed coronal-hole plasma

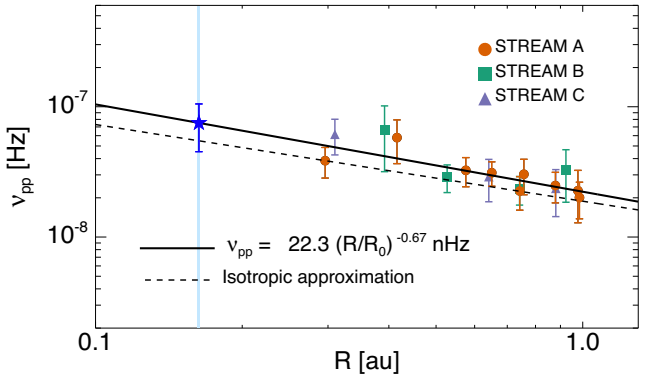

Figure 6. Radial dependence of the proton–proton collisional frequency. The legend is the same as in Fig. 5.

(i.e. originated from open magnetic field lines), we find a deviation from the generally accepted structure of the interplanetary magnetic field

$$|B_r| = (3.5 \pm 0.2)(R/R_0)^{-(1.81\pm0.08)}\ \mathrm{nT} \quad (3)$$

$$|B_t| = (2.9 \pm 0.2)(R/R_0)^{-(1.21\pm0.09)}\ \mathrm{nT} \quad (4)$$

with B_r decreasing more slowly than expected and B_t decreasing faster (not shown here). Alfvénic fluctuations dominate these high-speed intervals that, due to their large amplitude and not linearly polarized characteristics, tend to preferentially reduce the radial fluctuations with respect to the background state (Matteini et al. 2015). As a consequence, the radial behaviour of B_r could be due to a combination of a mean part in accordance with the Parker spiral and a fluctuating part with a different scaling.

3.2 Temperature

Fig. 5(c) displays the radial dependence of the total proton-core temperature

$$T_\mathrm{p} = (1.9 \pm 0.1) \times 10^5 (R/R_0)^{-(0.9\pm0.1)}\ \mathrm{K} \quad (5)$$

that decreases more slowly with respect to the adiabatic prediction. By considering a steady state, spherically expanding solar wind with a radially constant speed, a number density profile varying as R^{-2} and a negligible proton heat flux, the radial behaviour for the net volumetric heating rate (Breech et al. 2010) is $Q_\mathrm{p} \propto R^{-(3.9\pm0.2)}$, in agreement with previous studies (e.g. Hellinger et al. 2011). However, the profile of T_p decreases faster than in Hellinger et al. (2011), where $T_\mathrm{p} \propto R^{-0.74}$ (black-dashed line). Moreover, the contribution of parallel and perpendicular temperature (not shown here) is

$$T_\parallel = (1.2 \pm 0.1) \times 10^5 (R/R_0)^{-(0.5\pm0.1)}\ \mathrm{K} \quad (6)$$

$$T_\perp = (2.3 \pm 0.1) \times 10^5 (R/R_0)^{-(1.0\pm0.1)}\ \mathrm{K} \quad (7)$$

while Hellinger et al. (2011) found $T_{\shortparallel} \propto R^{-0.54}$ and $T_\perp \propto R^{-0.83}$, respectively. The evolution of $T_{\shortparallel}$ is consistent but that of $T_\perp$ is not.

The temperature anisotropy decreases with distance as shown in Fig. 5(d):

$$T_\perp/T_\parallel = (2.1 \pm 0.1)(R/R_0)^{-(0.41\pm0.08)} \quad (8)$$

still remaining larger than 1 at 1 au. Based on the $\beta_{\shortparallel}$ values in stream A, we can estimate, at different radial distances, the expected average threshold values of the temperature anisotropy for the cyclotron and mirror-mode instabilities (Hellinger et al. 2006), and for the empirical relation found by Marsch, Ao & Tu (2004). The results of the linear fit for the thresholds are also shown in Fig. 5(d), as an indication for a possible wave–particle interaction deriving from plasma instabilities. In agreement with Hellinger et al. (2006), the measured anisotropies are constrained by the mirror mode instability (pink-dot–dashed line), but the best agreement is found by using the anticorrelation proposed by Marsch et al. (2004) (black-dotted line), which follows closely the fit of $T_\perp/T_{\shortparallel}$. Finally, the values of temperature anisotropy do not seem to be limited by the proton cyclotron instability threshold (blue-dashed line).

The presence of perpendicular heating can be also confirmed by the direct analysis of the radial evolution of the adiabatic invariants (not shown here). In particular, for the proton magnetic moment, we find

$$T_\perp/B = \mu_\mathrm{p} \propto (R/R_0)^{(0.6\pm0.1)}. \quad (9)$$

This is in agreement with the least-squares fit index (∼0.6) found by Marsch et al. (1983) in the range of velocity [700, 800] km s^{-1}. In contrast, the fit for the second invariant is

$$T_\parallel (B/n)^2 \propto (R/R_0)^{(0.2\pm0.3)}, \quad (10)$$

where the large error, probably due to the larger uncertainty on the parallel temperature, does not allow us to make conclusions about its conservation. Indeed, Marsch et al. (1983) found that the curve was almost flat in fast wind. Finally, we consider another invariant, $T_{\shortparallel}(T_\perp/n)^2$, which is independent of the three-dimensional structure of the interplanetary magnetic field, under the assumption that energy sources and sink terms can be discarded, and we obtain

$$T_\parallel (T_\perp/n)^2 \propto (R/R_0)^{(1.4\pm0.4)} \quad (11)$$

in agreement with the behaviour observed by Marsch et al. (1983) in the velocity range [700, 800] km s^{-1}. Therefore, since at least one of the double-adiabatic invariants are observed to be broken, this confirms the action of dissipation or collisions.

To conclude the study of the thermodynamics of the fast wind, the proton kinetic and magnetic pressure radial dependences (not shown here) are

$$P_\mathrm{k} = (0.0065 \pm 0.0005)(R/R_0)^{-(2.9\pm0.1)}\ \mathrm{nPa} \quad (12)$$

$$P_\mathrm{B} = (0.0131 \pm 0.0009)(R/R_0)^{-(3.2\pm0.1)}\ \mathrm{nPa}. \quad (13)$$

The faster decrease of the magnetic than kinetic pressure is reflected in the radial proton plasma beta variation

$$\beta_\mathrm{p} = P_\mathrm{k}/P_\mathrm{B} = (0.55 \pm 0.04)(R/R_0)^{(0.4\pm0.1)}. \quad (14)$$

The behaviour of the parallel proton plasma beta is similar

$$\beta_\parallel = (0.37 \pm 0.03)(R/R_0)^{(0.8\pm0.1)}. \quad (15)$$

3.3 Collisional frequency

Collisional processes could play an important role in the dynamics of the solar wind (e.g. Maruca et al. 2013). Here, we calculate the average collisional frequency of the proton-core population, ν_{pp}, for a single bi-Maxwellian. Following Hellinger (2016), the isotropization frequency is defined through the collisional evolution equations for parallel and perpendicular temperatures. The functional form of ν_{pp}, for relaxation of the perpendicular anisotropy ($T_\perp > T_{\shortparallel}$) in a

gyrotropic ionized gas by Coulomb self-collisions, is (Kogan 1961)

$$\nu_{pp} = \frac{2\sqrt{\pi}e^4 n_p \lambda}{m_p^{1/2}(k_B T_\parallel)^{3/2}} A^{-2} \left[-3 + (A+3)\frac{\tan^{-1}\sqrt{A}}{\sqrt{A}} \right], \quad (16)$$

where $A = T_\perp/T_\parallel - 1$ and λ is the Coulomb logarithm (Chhiber et al. 2016). The radial evolution of ν_{pp} is shown in Fig. 6, where the fit (black-solid line) is

$$\nu_{pp} = (22.3 \pm 2.2) \times 10^{-9} (R/R_0)^{-(0.7\pm0.2)} \text{ s}^{-1}. \quad (17)$$

This decreases monotonically with distance, although we observe a small bump between 0.3 and 0.4 au (corresponding to both an increase in density and a depression in temperature). For reference, we plot also the radial evolution of ν_{pp} but in an isotropic approximation (we assume that the isotropic temperature is equal to T_p), defined as $\bar{\nu}_{pp} = 1.9 \times 10^{-8} n_p \lambda T_p^{-3/2}$ s^{-1}, whose fit (black-dashed line) is

$$\bar{\nu}_{pp} = (18.8 \pm 1.9) \times 10^{-9} (R/R_0)^{-(0.6\pm0.2)} \text{ s}^{-1}. \quad (18)$$

The behaviour is the same but ν_{pp} decreases faster than $\bar{\nu}_{pp}$.

4 DISCUSSIONS AND CONCLUSIONS

We have presented a detailed analysis of the radial evolution of pure fast solar wind from 0.3 au ($\sim 60 R_s$) to the Earth, by using re-processed proton-core HELIOS data, meaning that a possible influence of the proton-beam is avoided. In contrast, previous studies did not separate the contribution of the two proton populations. In particular, Hellinger et al. (2011) used numerical moments of the proton distribution function instead of analytical fits; while e.g. in Marsch et al. (1982), although a fit to isolate the two proton populations is used, the radial trends are given by considering the full velocity distribution. The contribution of a secondary proton beam could explain the differences with our results.

Another important difference with previous studies is that, here, we focused on unperturbed plasma from coronal holes. The selection method, based on density, velocity, magnetic field, and proton specific entropy (Borovsky 2016), allows us to avoid the interaction regions, which represent an external source of heating and compression. In fact, if the choice of fast intervals, e.g. for stream A, is done only by inspection of the plasma speed (i.e. the interval is considered between the highest value of the velocity after the abrupt increase and the value before the systematically decrease), we find a change in the radial evolution of the stream that confirms the presence of compressed regions, e.g. the density decreases as $R^{-1.92}$ instead of $R^{-1.98}$ when we fit all the points. Moreover, we have tried to apply the threshold of $V > 600$ km s^{-1}, as in Hellinger et al. (2011), on the 2 yr of HELIOS data considered in the present analysis and we found slight differences with respect to the unperturbed intervals. However, when the threshold is applied to many years of solar-wind data (Stansby et al. 2018), the results are similar to Hellinger et al. (2011) (even if some differences can be due to the presence of the proton beam). Therefore, although the threshold in velocity could be a good approximation for the choice of fast stream in case of short intervals, it might become limited and misleading in case of large statistical datasets.

The other idea of the present analysis is to follow well-defined streams during several solar rotations and at different distances from the Sun, with the assumption that the coronal holes, where these streams originated, were stable in time. Recently, Heinemann et al. (2018) have shown that the properties of high-speed streams (especially the proton-bulk velocity) measured at 1 au are affected by the evolution of coronal holes in the solar atmosphere. However, their analysis is based on the observation of a well-observed, long-lived and low-latitude coronal hole in 2012, corresponding to maximum of solar activity. In our analysis, we considered a period of solar minimum, where the behaviour of the magnetic field on the Sun should be more regular and stable. Unfortunately, no data from the solar atmosphere are available to study the evolution of coronal holes. However, to have an idea of the overall evolution of the high-speed streams, it is possible to use data from IMP8 satellite as a reference at a fixed distance (i.e. 1 au) complementary to the HELIOS satellites. The comparisons (not shown here) confirm that the coronal holes are almost stable, since no strong change in the properties of the streams are observed. Therefore, we can conclude that in our intervals we are only sensitive to the radial, and not temporal, evolution of the unperturbed coronal-hole plasma.

Table 2. Comparison of the radial-evolution indices in fast solar wind. No information about the error are given in some of the previous analyses. The data for the unperturbed coronal-hole plasma are from stream A in Table 1.

	Radial evolution index		
	Unperturbed coronal-hole plasma	Fast wind $V > 600$ km s^{-1} Hellinger et al. (2011)	Fast wind speed range [700, 800] km s^{-1}[a]
n_p	-1.96 ± 0.07	-1.8	-1.88 ± 0.23
B	-1.59 ± 0.06	-1.6	-1.45 ± 0.20
T_p	-0.93 ± 0.10	-0.74	-0.86 ± 0.28
$T_\parallel$	-0.53 ± 0.13	-0.54	-0.69
$T_\perp$	-1.01 ± 0.10	-0.83	-1.17
$T_\perp/B$	0.59 ± 0.10	–	0.6
$T_\parallel(B/n)^2$	0.21 ± 0.26	–	$\sim$const
$T_\parallel(T_\perp/n)^2$	1.36 ± 0.35	–	0.6
β_p	0.36 ± 0.13	–	0.61 ± 0.18
$\beta_\parallel$	0.81 ± 0.14	1.91 ± 2.55[b]	–

Notes. [a]Different references have been used for comparison. In particular, the parameters with the error are from (Totten, Freeman & Arya 1995), while the others are from Marsch et al. (1982) and Marsch et al. (1983). [b]This value is from Marsch & Richter (1984).

The results of our analysis on the radial evolution of 9 unperturbed high-speed intervals from a specific coronal hole (i.e. stream A in Table 1) is reported in Table 2, where a comparison with previous analyses in fast wind is given. In particular, we found that the proton density decreases as expected for a stationary radially expanding plasma, $n_p \propto R^{-2}$, while previous analyses have shown a slower decrease (e.g. Hellinger et al. 2011), probably due to the presence of both secondary proton beams and interaction regions between fast and slow wind. On the other hand, we recovered the same behaviour for the magnetic field. However, by looking in detail at the evolution of the magnetic components, we found a deviation from the Parker prediction, with the radial component decreasing more slowly and the tangential component decreasing faster than expected. It is worth noting that radial evolution predicted by the Parker model (Parker 1958, 1963) are often used to make extrapolations about the magnetic field from one heliocentric distance to another as, for example, in space weather models (e.g. Riley, Linker & Arge 2014).

The 'failure' of the Parker prediction has been already reported in previous studies of *in situ* measurements from different missions (e.g. Lockwood, Owens & Rouillard 2009; Khabarova & Obridko 2012), with effects on the solar-wind outflow (Khabarova et al. 2018). In particular, several works were dedicated to study the slower decrease of B_r, implying to an excess of the magnetic flux, and many explanations, from kinematic effects to wrong averag-

ing methods, were suggested (Lockwood et al. 2009; Smith 2011; Lockwood & Owens 2013). Recently, Khabarova & Obridko (2012) found, by using multi-spacecraft hourly averaged data of magnetic field between 0.29 and 5 au, that $|B_r| \propto R^{-1.666}$ and $|B_t| \propto R^{-1.096}$, showing a stronger deviation for B_r than in our analysis. However, Khabarova & Obridko (2012) selected the intervals in accordance with the radial distance; therefore, the data include both slow and fast wind and interaction regions. Their results suggest that turbulent processes in the inner heliosphere may significantly influence the expansion of the magnetic field, an idea already proposed by different authors (e.g. Ragot 2006). In particular, they propose a quasi-continuous magnetic reconnection, occurring at the large-scale heliospheric current sheet as well as at small-scale current sheets during the solar-wind expansion, as a key process responsible for breaking the expected magnetic field radial dependence law.

Furthermore, we observed a perpendicular heating in the proton-core population, with a violation of the double-adiabatic invariants and a corresponding increase of entropy, in agreement with previous studies (although different indices are recovered). We also studied the perpendicular heating through the evolution of the proton-core temperature anisotropy and we found that it is constrained in the radial expansion by the mirror-mode instability, consistent with Hellinger et al. (2006). However, the best agreement is found with the empirical relation proposed by Marsch et al. (2004). Finally, no constraint from the proton-cyclotron instability is found. As pointed out by Isenberg, Maruca & Kasper (2013), this result could be due to the estimation of the anisotropy threshold under the assumption that the proton distribution function is a bi-Maxwellian. In fact, resonant interactions between ion cyclotron waves and collisionless protons never yields bi-Maxwellian distributions. However, the instability thresholds used in the present study are based on an electron–proton plasma (Hellinger et al. 2006), while Matteini et al. (2007) have shown that the observations can be compatible with the proton-cyclotron instability constraints, when alpha particles are included in the model. The study of the stability conditions for an electron–proton–alpha plasma in the inner heliosphere will be presented in a future work (Stansby et al. 2018).

Finally, we observed that the behaviour of the collisional frequency for a bi-Maxwellian distribution is to decrease as the plasma moves away from the Sun. Moreover, comparing ν_{pp} with its isotropic approximation we found a faster decrease and larger local values, in agreement with numerical experiments where an increase of plasma collisionality due to velocity space deformations of the ion distribution functions is recovered (Pezzi, Valentini & Veltri 2016; Pezzi 2017). We have extrapolated the collisional time-scale, τ, as the inverse of $\bar{\nu}_{pp}$, to 0.1 au to be compared with the studies performed by Chhiber et al. (2016). They used a three-dimensional magnetohydrodynamic simulation of the global heliosphere to improve the estimation of the collisional time during the solar wind expansion by means of the self-collisional time defined in Spitzer (1956). We found $\sim 1.4 \times 10^7$ s, larger than the value found in Chhiber et al. (2016) ($\sim 10^6$ s, Fig. 1), suggesting that their model overestimates the collisionality.

Finally, we point out that our conclusions are almost independent, in the limit of the error, of the specific coronal-hole source. In this respect, in Table 3 we summarize the radial dependence (power-law index and expected value at 1 au) for all the parameters evaluated in our study.

Observations of fast solar wind from the three orbits of the Ulysses mission have shown that energy flux and particle flux are regulated by the amount of magnetic flux that opens into the heliosphere (Schwadron and McComas 2008). Parker Solar Probe and Solar Orbiter will give an important contribution to look for secular changes. The knowledge of how plasma from coronal holes evolves between 0.3 and 1 au allows us to predict the high-speed solar-wind environment much closer to the Sun, which Parker Solar Probe will eventually explore in the near future. During the first three perihelia (until 2019 September), Parker Solar Probe will take measurements of the solar wind at heliocentric distance of 0.163 au ($\sim 35 R_s$), before approaching the Alfvén critical point. In Table 4 we estimate the characteristic mean values of fast solar-wind plasma at the distance of $35 R_s$ by using the radial trends in Table 3. These results are in agreement with the general picture of the fast wind evolution from the corona to the heliosphere described in (Cranmer 2002), by using both remote sensing and *in situ* observations. However, the extrapolation of characteristic values, by using the power laws estimated between 0.3 and 1 au, can be reliable only far from the critical sound and Alfvén regions, where different physical processes could be at work. Therefore, a quantitative comparison with coronal observations is not currently possible. Only Solar Orbiter will provide an insight into the problem of the origin for different streams. Finally, in the near future, thanks to both Parker Solar Probe and Solar Orbiter, it will be possible to have a complete description of the plasma state of the corona and solar wind.

Table 3. Summary of the fitting for the radial profile of unperturbed high-speed coronal-hole plasma, $f = f_0(R/1\,\mathrm{au})^{\alpha}$. All the intervals listed in Table 1 are used together independently of their origin.

Unperturbed coronal-hole plasma evolution		
	f_0	α
n_p (cm^{-3})	2.37 ± 0.08	− 2.02 ± 0.05
$n_p V_r$ (10^3 cm^{-3} km s^{-1})	1.53 ± 0.05	− 1.99 ± 0.05
B (nT)	5.6 ± 0.1	− 1.63 ± 0.03
$\lvert B_r\rvert$ (nT)	3.5 ± 0.1	− 1.84 ± 0.05
$\lvert B_t\rvert$ (nT)	2.9 ± 0.1	− 1.29 ± 0.06
T_p (10^5K)	1.96 ± 0.09	− 0.90 ± 0.08
$T_{\parallel}$ (10^5 K)	1.29 ± 0.07	− 0.48 ± 0.09
$T_{\perp}$ (10^5 K)	2.3 ± 0.1	− 0.99 ± 0.08
$T_{\perp}/T_{\parallel}$	2.02 ± 0.07	− 0.43 ± 0.06
$T_{\perp}/B$ (10^4 K nT^{-1})	4.2 ± 0.2	0.65 ± 0.08
$T_{\parallel}(B/n)^2$ (10^5 KnT^{2}cm^6)	7.6 ± 0.7	0.3 ± 0.2
$T_{\parallel}(T_{\perp}/n)^2$ (10^{15} K^{3}cm^6)	1.4 ± 0.2	1.6 ± 0.3
ν_{pp} (nHz)	22 ± 2	− 0.8 ± 0.1
S_p (eV cm^2)	9.6 ± 0.5	0.45 ± 0.09
P_k (10^{-11} Pa)	0.66 ± 0.04	− 2.89 ± 0.09
P_B (10^{-11} Pa)	1.30 ± 0.06	− 3.23 ± 0.07
β_p	0.56 ± 0.03	0.40 ± 0.08
$\beta_{\parallel}$	0.40 ± 0.03	0.9 ± 0.1

Table 4. Prediction for fast solar wind during the first three perihelia of Parker Solar Probe.

Unperturbed coronal-hole plasma at $35R_s$		
B	$\lvert B_r\rvert$	$\lvert B_t\rvert$
(108 ± 9) nT	(99 ± 11) nT	(30 ± 4) nT
T_p	$T_{\perp}$	$T_{\parallel}$
(10 ± 2) 10^5 K	(14 ± 3) 10^5 K	(3.1 ± 0.7) 10^5 K
n_p	ν_{pp}	β_p
(92 ± 12) cm^{-3}	(9 ± 3) 10^{-8} Hz	(0.31 ± 0.04) nHz
P_k	P_B	$\beta_{\parallel}$
(1.3 ± 0.3) nPa	(4.6 ± 0.8) nPa	(0.08 ± 0.01)

ACKNOWLEDGEMENTS

Work by DP and TSH was supported by STFC grant ST/N000692/1; DS was supported by a studentship under STFC grant ST/N504336/1; and LM was supported by the Programme National PNST of CNRS/INSU co-funded by CNES.

REFERENCES

Bavassano B., Dobrowolny M., Fanfoni G., Mariani F., Ness N. F., 1982b, Solar Phys., 78, 373
Bavassano B., Dobrowolny M., Mariani F., Ness N. F., 1981, J. Geophys. Res., 86, 1271
Bavassano B., Dobrowolny M., Mariani F., Ness N. F., 1982a, J. Geophys. Res., 87, 3617
Borovsky J. E., 2016, J. Geophys. Res., 121, 5055
Bourouaine S., Marsch E., Neubauer F. M., 2010, Geophys. Res. Lett., 37, L14104
Breech B., Cranmer S. R., Matthaeus W. H., Kasper J. C., Oughton S., 2010 , in AIP Conf. Proc. Vol. 1216. Am. Inst. Phys., New York, p. 214
Breech B., Matthaeus W. H., Cranmer S. R., Kasper J. C., Oughton S., 2009, J. Geophys. Res., 114, A09103
Camporeale E., Carè A., Borovsky J. E., 2018, J. Geophys. Res., 122, 10910
Chew G. F., Goldberger M. L., Low F. E., 1956, Proc. R. Soc. A, 236, 112
Chhiber R., Usmanov A. V., Matthaeus W. H., Goldstein M. L., 2016, ApJ, 821, 34
Cranmer S. R., 2002, Space Sci. Rev., 101, 229
Cranmer S. R., Matthaeus W. H., Breech B. A., Kasper J. C., 2009, ApJ, 702, 1604
Fox N. J. et al., 2016, Space Sci. Rev., 204, 7
Gary S. P., Skoug R. M., Steinberg J. T., Smith C. W., 2001, Geophys. Res. Lett., 28, 2759
Geiss J., Gloeckler G., Von Steiger R., 1995, Space Sci. Rev., 72, 49
Heinemann S. G., Temmer M., Hofmeister S. J., Veronig A. M., Vennerstrom S., 2018, ApJ, 861, 151
Hellinger P., 2016, ApJ, 825, 120
Hellinger P., Matteini L., Stverák S., Trávnícek P. M., Marsch E., 2011, J. Geophys. Res., 116, A09105
Hellinger P., Trávnícek P. M., Kasper J. C., Lazarus A. J., 2006, Geophys. Res. Lett., 33, L09101
Hellinger P., Trávnícek P. M., Stverák S., Matteini L., Velli M., 2013, J. Geophys. Res., 118, 1351
Heuer M., Marsch E., 2007, J. Geophys. Res., 112, A03102
Hollweg J. V., Isenberg P. A., 2002, J. Geophys. Res., 107, 1147
Horbury T. S., Matteini L., Stansby D., 2018, MNRAS, 478, 1980
Hundhausen A. J., 1972, Coronal Expansion and Solar Wind. Springer-Verlag, Berlin, Heidelberg
Isenberg P. A., Maruca B. A., Kasper J. C., 2013, ApJ, 773, 164
Khabarova O. V., Obridko V. N., 2012, ApJ, 761, 82
Khabarova O. V., Obridko V. N., Kislov R. A., Malova H. V., Bemporad A., Zelenyi L. M., Kuznetsov V. D., Kharshiladze A. F., 2018, Plasma Phys. Rep., 44, 840
Kogan V., I., 1961, in Leontovich M. A., eds, Plasma Physics and the Problem of Controlled Thermonuclear Reactions, Vol. 1. Pergamon, New York
Livi S., Marsch E., Rosenbauer H., 1986, J. Geophys. Res., 91, 8045
Lockwood M., Owens M., Rouillard A. P., 2009, J. Geophys. Res., 114, A11104
Lockwood M., Owens M. J., 2013, J. Geophys. Res., 118, 1880
Marsch E., Ao X.-Z., Tu C.-Y., 2004, J. Geophys. Res., 109, A04102
Marsch E., Goldstein H., 1983, J. Geophys. Res., 88, 9933
Marsch E., Muhlhauser K.-H., Rosenbauer H., Schwenn R., 1983, J. Geophys. Res., 88, 2982
Marsch E., Muhlhauser K.-H., Schwenn R., Rosenbauer H., Pilipp W., Neubauer F. M., 1982, J. Geophys. Res., 87, 52
Marsch E., Richter A. K., 1984, J. Geophys. Res., 89, 6599
Marsch E., Richter A. K., 1987, Ann. Geophys., 5, 71
Maruca B. A., Bale S. D., Sorriso-Valvo L., Kasper J. C., Stevens M. L., 2013, Phys. Rev. Lett., 111, 241101
Matteini L., Hellinger P., Landi S., Trávnícek P. M., Velli M., 2012, Space Sci. Rev., 172, 373
Matteini L., Horbury T. S., Neugebauer M., Goldstein B. E., 2014, Geophys. Res. Lett., 41, 259
Matteini L., Horbury T. S., Pantellini F., Velli M., Schwartz S. J., 2015, ApJ, 802, 11
Matteini L., Landi S., Hellinger P., Pantellini F., Maksimovic M., Velli M., Goldstein B. E., Marsch E., 2007, Geophys. Res. Lett., 34, L20105
Muller D., Marsden R. G., St. Cyr O. C., Gilbert H. R., 2013, Solar Phys., 285, 25
Parker E. N., 1958, ApJ, 128, 664
Parker E. N., 1963, Interplanetary Dynamical Processes. Interscience, New York
Pezzi O., 2017, J. Plasma Phys., 83, 555830301
Pezzi O., Valentini F., Veltri P., 2016, Phys. Rev. Lett., 116, 145001
Ragot B. R., 2006, ApJ, 651, 1209
Richardson I. G., 2018, Living Rev. Solar Phys., 15, 1
Riley P., Linker J. A., Arge C. N., 2014, Space Weather, 13, 154
Schwadron N. A., McComas D. J., 2008, ApJ, 686, L33
Schwenn R., Marsch E., 1990, Physics of the Inner Heliosphere. I: Large-Scale Phenomena. Springer-Verlag, Berlin, Heidelberg
Smith E. J., 2011, J. Geophys. Res., 116, A12101
Spitzer L., 1956, *Physics of Fully Ionized Gases*, Interscience Tracts on Physics and Astronomy, Vol. 3. Interscience, New York
Stansby D., 2017, Helios proton core parameter dataset, Available at: http://doi.org/10.5281/zenodo.1009506
Stansby D., Horbury T. S., Matteini L., 2019, MNRAS, 482, 1706
Stansby D., Perrone D., Matteini L., Horbury T. S., Salem C. S., 2018, A&A, preprint (arXiv:1812.06881)
Stansby D., Salem C., Matteini L., Horbury T., 2018, Solar Phys., 293, 155
Totten T. L., Freeman J. W., Arya S., 1995, J. Geophys. Res., 100, 13

This paper has been typeset from a TEX/LATEX file prepared by the author.